Super spin-glass state in two-dimensional aggregated Fe_3O_4 nanoparticles deposited on a plasma-treated polymeric substrate

M. Orendáč,[1,2] S. Lupínková,[3] A. Doroshenko,[1,*] E. Čižmár,[1] A. Orendáčová,[1] V. Švorčík,[2] O. Lyutakov,[2] D. Fajstavr,[2] Z. Kolská,[3] A. Zeleňáková,[1] and D. Peddis[4]

[1]*Institute of Physics, P. J. Šafárik University in Košice, Park Angelinum 9, 040 01, Košice, Slovak Republic*

[2]*Department of Solid State Engineering, University of Chemistry and Technology, Technická 5, Prague 16628, Czech Republic*

[3]*Faculty of Science, J. E. Purkyně University, Pasteurova 3544/1, 400 96, Ústí nad Labem, Czech Republic*

[4]*Department of Chemistry and Industrial Chemistry, University of Genova, Via Dodecaneso 31 16146, Genova, Italy and ISM-CNR, Via Salaria, Km 29, 300 00015 Monterotondo Scalo, Roma, Italy*

(Received 28 March 2023; revised 10 July 2023; accepted 5 September 2023; published 26 September 2023)

The assembly consisting of Fe_3O_4 nanoparticles deposited on a plasma-treated polypropylene substrate was structurally characterized and its static and dynamic magnetic properties were investigated. The Fe_3O_4 nanoparticles of the nominal size of 10 nm create agglomerates of the size ranging from nominally 10 to 400 nm which were deposited on the polypropylene substrate using the grafting technique. The behavior of zero field cooled and field cooled susceptibility was found to be consistent with the onset of the super spin-glass state with glassy temperature $T_g = 211$ K. The formation of the super spin-glass state was also supported by the relative shift of maximum in alternating susceptibility $\Gamma \approx 0.06$ and $z\varepsilon = 8.6$ obtained from critical slowing down analysis as well as by the study of memory and aging effects. Significant renormalization of T_g and $z\upsilon$ for obtaining universal behavior in dynamic scaling of alternating susceptibility is tentatively ascribed to deviation toward two-dimensional magnetic behavior. The obtained results suggest that the studied assembly may be appropriate for the realization of unique two-dimensional super spin glass with dominant dipolar interaction.

DOI: 10.1103/PhysRevB.108.104423

I. INTRODUCTION

Disordered systems are known to display phenomena coexisting at timescales ranging from those comparable with fluctuation of atoms in the lattice to processes lasting many years. This unique property results from an extremal width in their distribution function of the relaxation times. In magnetic disordered materials random interactions among magnetic moments may lead to the formation of the so-called spin-glass state. In archetypal spin glasses, the spin-glass state arises as a result of magnetic interactions among individual magnetic ions. However, magnetic single-domain cluster/nanoparticle systems (MNPs) may create *super* spin glass (SSG) as one of the possible *super* phases. The onset of the SSG state may significantly alter the magnetic response of an assembly in which it appears. For example, giant spontaneous exchange bias found in Sb doped Heusler alloy $Ni_{50}Mn_{38}Ga_{12}$ was attributed to the interaction of SSG and antiferromagnetic matrix in which crossover from the canonical spin glass to the cluster spin glass plays a key role [1]. The study of exchange coupled $[Dy/Tb]_{10}$ multilayers revealed the presence of SSG with superimposed helical magnetic configurations arising due to spin-frustrated interfaces. The coexistence of SSG and the helical states was proposed to be responsible for the topological stability of spin configurations in the studied rare-earth/rare-earth multilayers [2].

The formation and properties of SSG have been frequently investigated in the assembly of single-domain MNPs focusing on the conditions of SSG formation depending on the size, shape, and composition of the nanoparticles [3,4]. As anticipated, for ultrasmall MNPs (≈2 nm) surface states become important. A Monte Carlo study of interacting ultrasmall ferrimagnetic MNPs proved the correlation between SSG and the exchange bias which was attributed to the interplay between the intraparticle spin structure and the interparticle coupling [5]. Nonequilibrium dynamics of SSG in a dense assembly of nominally 2 nm $MnFe_2O_4$ nanoparticles confirmed memory and aging effects similar to those in archetypal spin glasses. The experimental results were reasonably reproduced by Monte Carlo simulations using a mesoscopic model of the MNP assembly with core/shell morphology as well as intraparticle (core, surface, core/surface interface) and interparticle (exchange, dipolar) couplings taken into account [6].

Regarding "manmade" structures, the critical behavior of two-dimensional (2D) arrays, which consisted of Ising nanomagnets lithographically arranged in random sites and angular orientations, was found to be close to that for a 2D Ising model in a square lattice. Enhancing randomness in nanomagnets' sizes and positions was proposed to shift the properties of the studied assembly toward glassy behavior [7]. In contrast, 2D arrays of regularly spaced nanomagnets proved to be successful in creating artificial spin ices [8]. In these systems, shape anisotropy defines Ising-like magnetic moments which obey local ice rules. The ice rules appear as a consequence of frustration arising due to the interplay of effective ferromagnetic coupling and the orientation of the local anisotropy

*Corresponding author: anastasiia.doroshenko@student.upjs.sk

axes, similarly as in the canonical spin ice [9]. On the other hand, randomness in the magnitude of magnetic couplings and/or coexistence of ferro- and antiferromagnetic bonds in the lattice represent a necessary prerequisite for the onset of spin-glass behavior.

Notably, even in archetypal spin glasses the relation between the potential transition to the spin-glass state and spatial anisotropy of exchange coupling and spin dimensionality as well as the type of distribution of the magnitudes of exchange coupling, hereafter denoted as J, has not been fully clarified yet. More specifically, the pioneering work of Sherrington and Kirkpatrick [10] adopting a mean-field approach for a simple three-dimensional (3D) Ising ferromagnet confirmed that even in such a system the spin-glass state may be formed for a sufficiently wide Gaussian distribution of J. Subsequent theoretical studies and Monte Carlo simulations confirmed that a 3D array of Ising spins with Gaussian distribution of the nearest neighbor interactions enters the spin-glass phase at nonzero critical temperature T_c, but the spin glass may exist only at $T_c = 0$ K for a 2D system [11,12]. On the other hand, for a 2D Ising spin glass with a bimodal distribution of exchange coupling ($\pm J$) the situation remains inconclusive since the predictions about the value of the critical temperatures differ depending on the details of the Monte Carlo technique used and the cluster size [13,14].

Experimentally, although a plethora of 3D spin glasses has been studied [15], the results for 2D systems are very scarce. For example, the nonlinear part of the static susceptibility of $Rb_2Cu_{1-x}Co_xF_4$ was found to obey scaling in accordance with the Edwards-Anderson model for a 2D ($\pm J$) Ising magnetic system [16] and the scaling yielded $T_c = 0$ K. Regarding 2D Heisenberg spin glasses, systematic studies of spin freezing in thin layers of CuMn and AgMn revealed nonzero freezing temperature even for one and two CuMn monolayers [17]. The obtained result suggested that 2D Heisenberg metallic spin glass with Ruderman-Kittel-Kasuya-Yosida (RKKY) interaction enters the spin-glass phase above absolute zero in contrast with the theoretical prediction for Heisenberg spin glasses with short-range interactions [18]. A recent neutron scattering study of 2D hybrid Heisenberg-Ising spin glass $Mn_{0.5}Fe_{0.5}PS_3$ revealed $T_c = 35$ K and spin configurations in which the energies of not all exchange paths within the honeycomb planes are satisfied due to geometrical frustration [19].

It should be stressed that all the aforementioned studies addressed SSG transition in magnetically 3D systems. To the best of our knowledge, the potential formation of SSG in a 2D system with dominant long-range dipolar interactions has not been theoretically and experimentally studied very thoroughly yet. In addition, the persisting lack of understanding of the formation of a spin-glass state upon altering spin anisotropy and tuning magnetic dimensionality from 3 to 2 suggests a need for systematic investigation of appropriate predominantly 2D structures. To this end, the assembly consisting of Fe_3O_4 nanoparticles deposited on a plasma-treated polypropylene substrate was designed and manufactured using the grafting technique. A schematic plot of the manufactured assembly is illustrated in Fig. 1.

SSG behavior may be anticipated, firstly, due to the distribution of magnitudes of dipolar interactions arising from the distributions of sizes of the agglomerates and their random locations on the substrate. Secondly, the random orientation of the anisotropy axes of the deposited nanoparticles and the presence of dipolar coupling may introduce frustration.

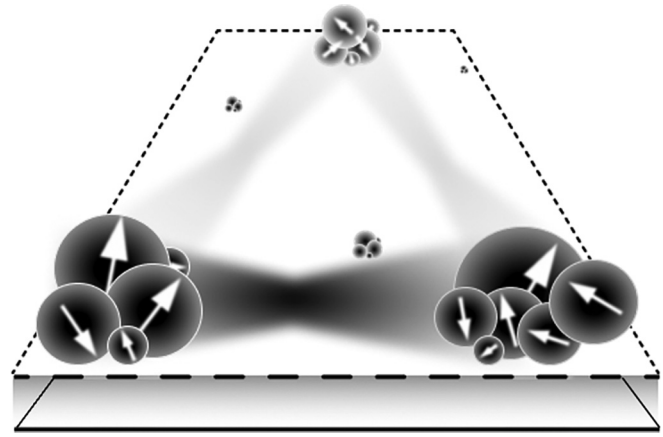

FIG. 1. Schematic plot of Fe_3O_4 nanoparticles deposited on plasma-treated polypropylene substrate. For simplicity, magnetic moments in only three aggregates and dipolar couplings among them are denoted by arrows and shaded areas, respectively.

Structural characterization showed that the assembly consists of aggregates with size distribution varying from ≈10 nm to nominally 400 nm of Fe_3O_4 nanoparticles of ≈10 nm mean size. Static and dynamic magnetic properties investigated in a wide range of temperatures and excitation frequencies using well-established protocols support the onset of the SSG state in the studied system.

II. EXPERIMENTAL DETAILS

A. Materials and modification

All chemicals used were of analytical grade without any further purification. Ferric chloride ($FeCl_3{\cdot}6H_2O$), ferrous chloride ($FeCl_2{\cdot}4H_2O$), and ammonia solution (32%) were purchased from Merck. Chitosan (medium molecular weight, deacetylation degree of 75%–85%) was purchased from Sigma-Aldrich.

The synthesis of the Fe_3O_4 MNPs was conducted according to the procedure previously reported [20]. The mixture of 1.0 g $FeCl_2{\cdot}4H_2O$ and 2.0 g $FeCl_3{\cdot}6H_2O$ salts in 90.0 ml of distilled water was placed in a conical flask under vigorous stirring; the appropriate amount of ammonia solution was added to the stirring mixture until the pH value was 11 and then it was stirred for 20 min at room temperature. Then Fe_3O_4 nanoparticles were centrifuged, washed thoroughly with distilled water, and redispersed in distilled water for further usage.

Biaxially oriented polypropylene (PP) in the form of 50 μm thick foils (supplied by Goodfellow Ltd., UK) was firstly treated in atmospheric plasma using a RPS40+ plasma device (Roplass, s.r.o., CZ) for 30 s with 75 W power.

The samples were immersed in a 0.1% chitosan solution immediately after the plasma treatment due to better adhesion of particles on the PP substrate [20]. After 24 h, the PP samples were removed from the solution, rinsed with distilled water, and inserted into an aqueous dispersion of Fe_3O_4

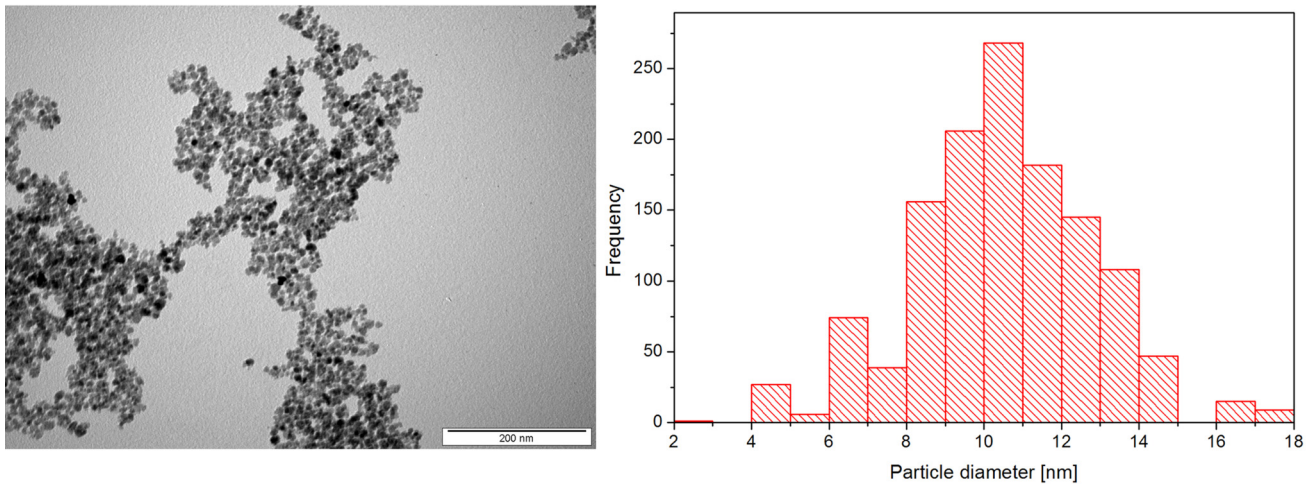

FIG. 2. TEM micrograph of Fe_3O_4 nanoparticles before their immobilization onto PP and their calculated size distribution.

nanoparticles for 24 h; after that they were rinsed again with distilled water and left to air dry.

B. Measurement techniques

The crystallographic structure of the prepared nanoparticles was characterized by x-ray diffraction analysis (XRD) using a PANanalytical X'Pert PRO x-ray diffractometer [20].

The structure and morphology of Fe_3O_4 MNPs were investigated by transmission electron microscopy (TEM). The JEOL JEM-1010 (JEOL Ltd., JP) transmission electron microscope was applied while the TEM images were recorded at the accelerating voltage of 80 kV.

Scanning electron microscopy (SEM, Lyra3 GMU, Tescan, CZ) was employed to study the surface morphology of Fe_3O_4 MNPs deposited on a PP surface. The accelerating voltage used was 10 kV. The substrate was coated with a 20 nm thick silver layer to prevent surface charging.

Particle size distributions were derived from TEM and SEM results by the analysis of the micrographs in the IMAGEJ program.

In order to investigate magnetic properties, the studied assembly was cut to the form of a stripe of 7 mm width and 12 cm length. To suppress the interlayer dipolar coupling the sample stripe was placed on a paper sheet of 100 μm thickness (size of 12 $\times$ 12 cm^2), wrapped into a cylindrical shape and fixed in the plastic straw. In such a way no contribution of supporting paper sheet and plastic straw to the total magnetic moment is detected using the commercial SQUID magnetometer Quantum Design MPMS3. Only a contribution of the PP stripe in addition to the Fe_3O_4 nanoparticle assembly needs to be accounted for, which proved to be negligible in a separate measurement run with a pure PP stripe. The static susceptibility was calculated as the ratio of measured magnetic moment and applied magnetic field, $\chi = M/H$. A more detailed description of the used protocols is given in subsequent sections. The initial part of each protocol involved heating the sample to room temperature and resetting the superconducting magnet. Performing this step enabled us to keep the resultant remanent field smaller than 0.5 Oe.

III. RESULTS AND DISCUSSION

A. Material characterization

The XRD revealed that iron oxide particles prepared by the proposed procedure were in the form of magnetite (Fe_3O_4). More specifically, the resultant XRD spectrum contained only peaks which correspond to Fe_3O_4, marked with their indices (220), (311), (400), (422), (511), and (440) by comparison with the data from the ICSD PDF-2 database (see Fig. 1 in Ref. [20]). On the other hand, any peaks indicating a potential presence of impurity e.g., $Fe(OH)_3$ or Fe_2O_3, were absent. The average crystallite size of the iron oxide particles was calculated by the Scherrer equation to be about 9–10 nm [20]. It corresponds very well to the results obtained by TEM analysis.

The prepared nanoparticles have a spherical-like shape with an average diameter of around 10 nm (Fig. 2). It seems that Fe_3O_4 MNPs in the suspension tend strongly to agglomerate as a result of their large surface energy [21].

During immobilization of Fe_3O_4 nanoparticles onto a plasma-treated PP surface (Fe_3O_4-PP) a strong aggregation process has been observed (see Fig. 3). These aggregates are homogeneously distributed over the whole PP surface and have good adhesion to the surface, as they were not washed away during the rinsing process. The size of aggregates spans from 10 to 400 nm. The wide distribution of aggregates enables us to anticipate a wide distribution of the magnitudes of dipolar coupling which may represent an important condition for the onset of the SSG state.

B. Magnetic properties

1. Static susceptibility

Temperature dependence of static susceptibility was studied in standard zero field cooled (ZFC) and field cooled (FC) regimes in the temperature range 5−300 K in magnetic fields up to 1500 Oe; Fig. 4(a) displays the results for selected magnetic fields in the range 10–300 Oe, and Fig. 4(b) illustrates the data studied from 500 Oe to 1.5 kOe. Whereas FC susceptibility χ_{FC} monotonically increases upon cooling, ZFC susceptibility χ_{ZFC} displays a maximum at a

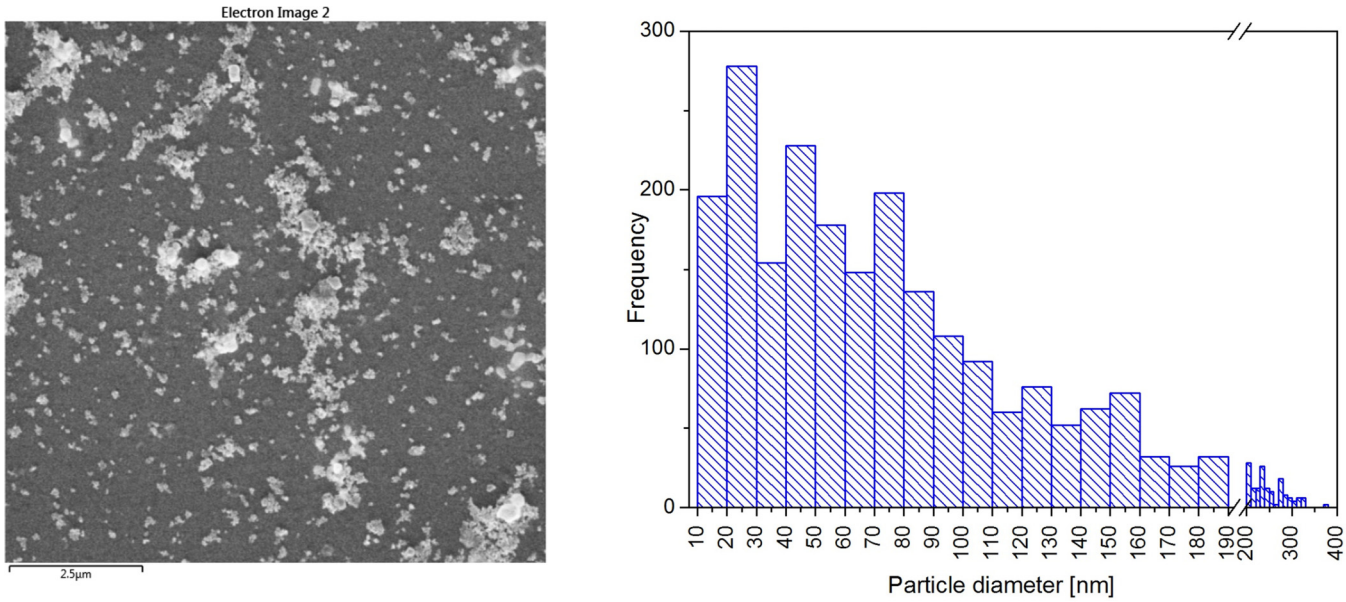

FIG. 3. SEM image of particles–aggregates of Fe_3O_4 nanoparticles–deposited on plasma-treated PP and their calculated size distribution.

temperature T_p, which is shifted toward lower values upon increasing the magnetic field. In addition, FC susceptibility curves tend to saturate for temperatures lower than T_p. While for magnetic fields lower than 50 Oe the temperature of bifurcation between ZC and ZFC susceptibility T_{irr} is significantly higher than T_p, the two temperatures become merged for magnetic fields higher than 300 Oe. The observed features in FC/ZFC susceptibility clearly indicate strong interactions among nanoparticles bringing the systems to an anistropy state at low temperature (i.e., temperature independent behavior of FC). Although the temperature dependence of ZFC susceptibility is qualitatively similar for a superparamagnet (SPM) and SSG, FC susceptibility becomes different. More specifically, in SPM at temperatures below T_p, although the superspins become blocked, the system still can be further polarized upon cooling. Consequently, FC susceptibility of SPM is characterized by a pronounced increase upon decreasing the temperature and the increase below T_p may reach even 80% as observed, e.g., in ferritin [22]. On the other hand, spin configurations in SSG are due to significant magnetic interactions that are much more robust against changing temperature. As a result, FC susceptibility of real SSG systems is becoming flat below T_p as reported, e.g., in Fe_3O_4 nanoparticles creating packed agglomerates [4] or slightly decreased with decreasing temperature as found in magnetically textured ferrofluid [23], Fe_3O_4 nanoparticles capped with a mixed monolayer of oleic acid and oleylamine [24], or $CoFe_2O_4$-SiO_2 nanocomposite [25]. Alternatively, the FC susceptibility below T_p can slightly increase in SSG systems as found in Fe_3O_4 nanoparticles prepared by the coprecipitation technique and coated by a SiO_2 layer [26], and bare Fe_3O_4 nanoparticles also prepared by the coprecipitation technique [27]. Similar behavior of FC susceptibility was revealed also in Fe_3O_4 monodispersed nanoparticles and an intercalated ensemble of nanoparticles and nanorods prepared by the coprecipitation technique, modified from those mentioned above, and both systems were identified as cluster glasses [28]. In contrast, although a slight tendency of gradual decreasing of FC susceptibility below T_p upon cooling was found in another system of Fe_3O_4 nanoparticles prepared by an alternative chemical method, the absence of the aging effect in the ZFC protocol does not support the SSG scenario [29]. Consequently, the behavior of FC susceptibility below T_p may serve as an indicative, but not decisive criterion for judging the onset of the SSG state. The presented data of ZFC susceptibility are consistent with interacting systems, and gradual merging of T_p and T_{irr} with the increasing magnetic field may suggest the formation of the SSG state [24]. However, a closer comparison of the FC and ZFC susceptibility data from Ref. [24] and those obtained for Fe_3O_4-PP suggest some striking differences. More specifically, in low magnetic fields the maximum in ZFC susceptibility in Fe_3O_4-PP is formed already above 200 K, whereas for the Fe_3O_4 nanoparticle system studied in Ref. [24] the corresponding maximum appears at nominally 30 K. This difference immediately suggests both T_{irr} and the glassy temperature associated with T_p are significantly higher in Fe_3O_4-PP. The observed feature may be associated with stronger magnetic coupling and a larger effective energy barrier in Fe_3O_4-PP arising predominantly due to larger Fe_3O_4 nanoparticles (10 nm in Fe_3O_4-PP vs 5.4 nm in those from Ref. [24]). In addition, ZFC susceptibility behavior reveals the $(T_{irr} - T_p)/T_{irr}$ ratio in Fe_3O_4-PP is much lower than that in the reference system, which might be related to different ratios of the effective energy barrier and the magnitude of effective dipolar interaction. Finaly, in Fe_3O_4-PP the value of T_p is much less robust against the change of the external magnetic field. The behavior can be quantitatively characterized by a relative change of T_p, $\Delta T_p/T_p$, with magnetic field, and this parameter for $\Delta H = 1500$ Oe yields the value 0.9 for Fe_3O_4-PP and 0.56 for the system from Ref. [24]. Consequently, quantitatively different critical behavior may be anticipated for the two systems. It is conceivable that the distribution

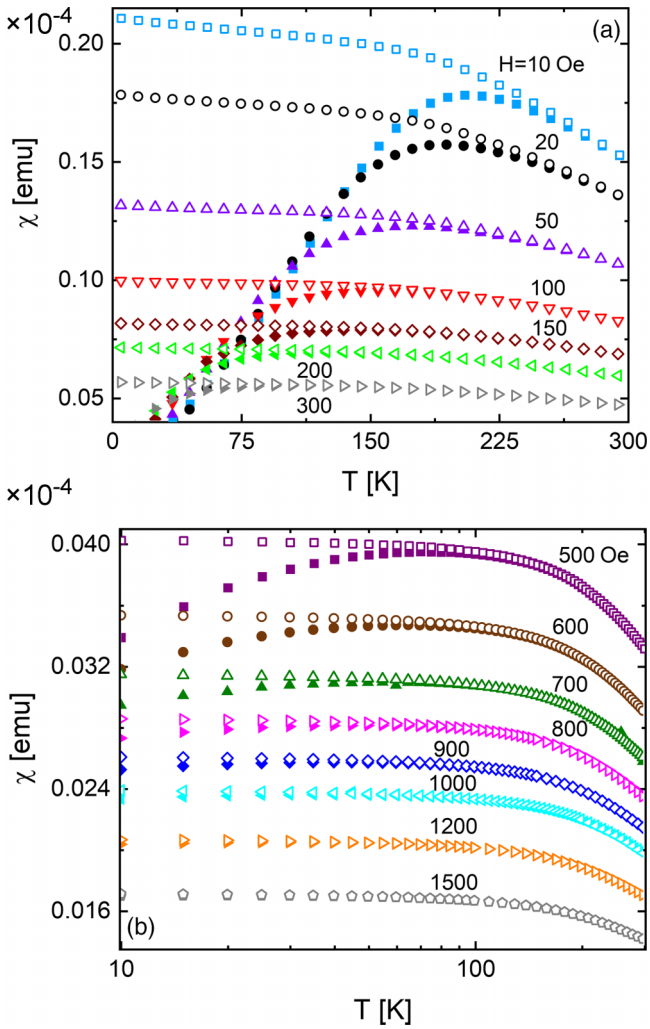

FIG. 4. (a) Temperature dependence of FC (open symbols) and ZFC (filled symbols) susceptibility of Fe_3O_4-PP at low magnetic fields used for the analysis of the critical line, 10 Oe (light blue squares), 20 Oe (black circles), 50 Oe (violet upward triangles), 100 (red downward triangles), 150 Oe (brown diamonds), 200 Oe (green left-pointing triangles), and 300 Oe (gray right-pointing triangles). (b) Temperature dependence of FC (open symbols) and ZFC (filled symbols) susceptibility of Fe_3O_4-PP at higher magnetic fields, 500 Oe (purple squares), 600 Oe (brown circles), 700 Oe (green upward triangles), 800 Oe (magenta right-pointing triangles), 900 Oe (blue diamonds), 1000 Oe (celeste right-pointing triangles), 1200 Oe (ochre right-pointing triangles), and 1500 Oe (gray pentagons). See the text for a more detailed discussion.

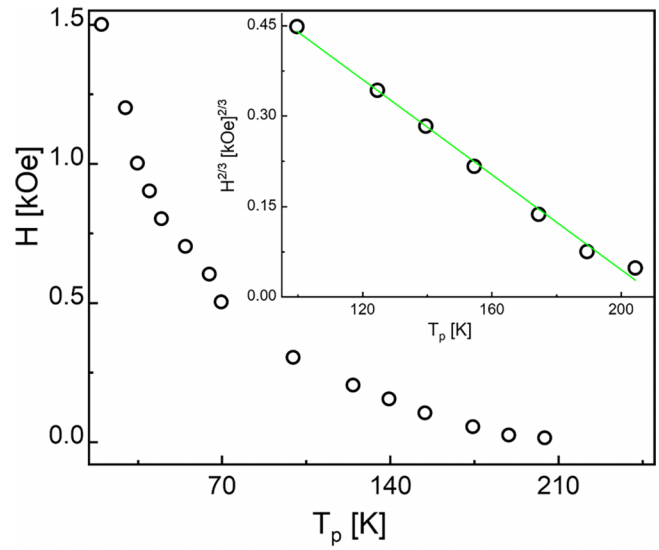

FIG. 5. Temperature dependence of the peak in ZFC susceptibility of Fe_3O_4-PP in various magnetic fields. Inset: Analysis of these data using Eq. (1); green solid line represents the result of the fit.

of the magnitudes of magnetic couplings and potentially different magnetic dimensionality may be responsible for the observed differences.

Quantitative analysis of the static susceptibility data can address the question about the existence of the phase boundary line between the SSG and SPM states. The existence of the phase boundary was predicted by de Almeida and Thouless using mean-field approximation for a 3D ferromagnetic system with Gaussian distribution of exchange coupling [30]. The phase boundary was proposed for low magnetic fields in the form

$$H(T_{AT}) = A[1 - T_{AT}(H)/T_{AT}(0)]^p, \quad (1)$$

in which $p = 3/2$; $T_{AT}(0)$ and $T_{AT}(H)$ represent the glass transition temperature in zero and nonzero magnetic field H, respectively. The constant A is related to the width of the distribution of exchange interactions. The determination of $T_{AT}(H)$ from the characteristic features of ZFC susceptibility data was systematically investigated in discontinuous $Co_{80}Fe_{20}/Al_2O_3$ multilayers [31]. More specifically, $T_{AT}(H)$ was successively associated with the inflection point in $\Delta\chi = \chi_{FC} - \chi_{ZFC}$ vs T dependence, the intersections of the steepest tangent of $\Delta\chi$ vs T, and the peak position in ZFC susceptibility. Adopting all three approaches led to very similar values of parameter p close to the predicted $p = 3/2$. Consequently, in the subsequent analysis, the phase boundary was constructed from the peak positions in ZFC susceptibility. This approach has also been used in studies of the SSG state in $La_{0.7}Sr_{0.3}MnO_3$ nanoparticles obtained by high-energy ball milling [32] and Fe_3O_4 nanoparticles capped with a mixed monolayer of oleic acid and oleylamine [24].

As can be seen in the inset of Fig. 5 very good agreement between the data and the prediction resulting from Eq. (1) was obtained for magnetic fields smaller than 300 Oe and the analysis yielded $T_{AT}(0) \equiv T_g = 211 \pm 2.2$ K and $A = 0.76 \pm 0.03$ Oe. It should be noted that for SPM the peak in the temperature dependence of ZFC susceptibility should scale with the magnetic field in the low-field region as H^2 [32,33]. Given that using the aforementioned approach led to very similar behavior of T_p vs H in other systems in which the spin-glass state or SSG were confirmed [24,34], the static susceptibility data of Fe_3O_4-PP seem to be consistent with the formation of SSG. However, the obtained values of both T_g and A should be accepted with caution since the wide distribution of the sizes of the aggregates enables us to foresee also a wide distribution of magnitudes of dipolar coupling, which is not suggested by the value of the A parameter. In contrast, the value of

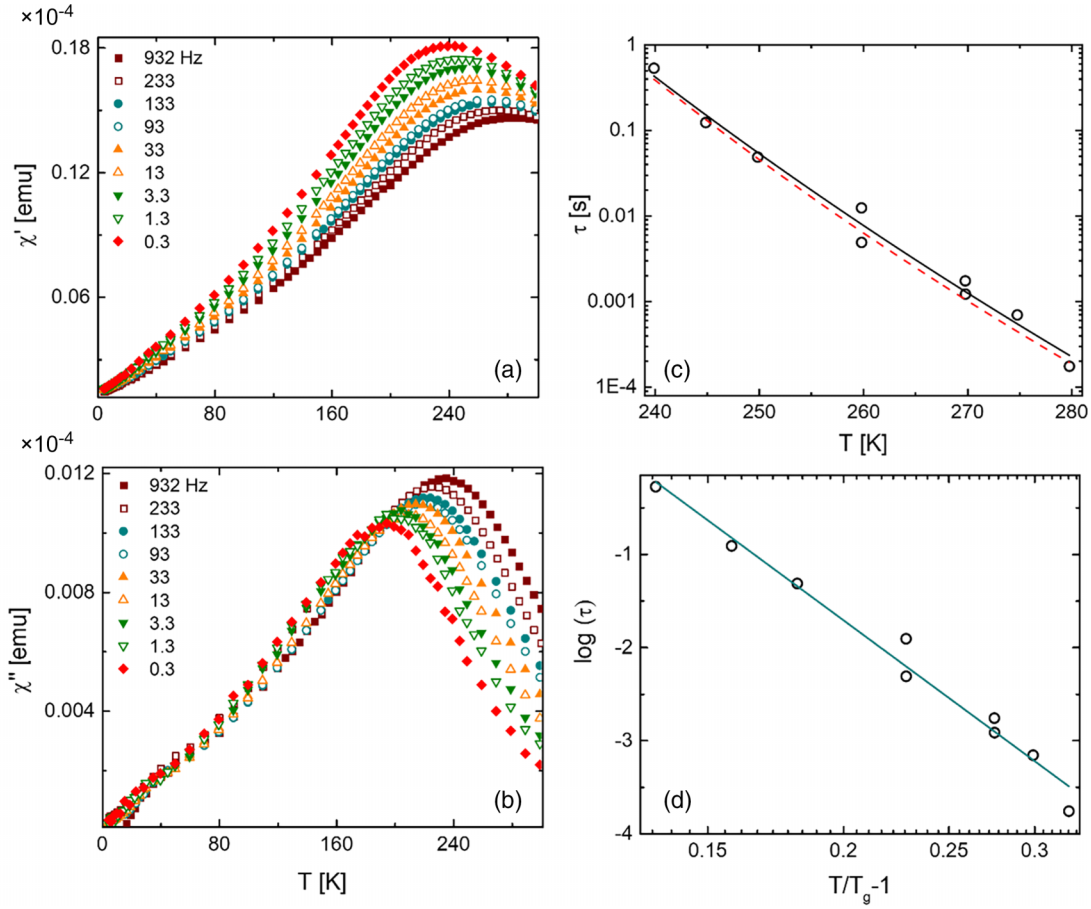

FIG. 6. Temperature dependence of (a) real and (b) imaginary susceptibility of Fe_3O_4-PP studied at various frequencies and zero static magnetic field. (c) The analysis of the temperature dependence of the relaxation time using the Arrhenius formula (red dashed line) and the prediction for a 2D Ising spin glass with bimodal exchange interactions (black solid line). (d) The analysis of the temperature dependence of the relaxation time using power law for critical slowing down.

the critical temperature seems to be overestimated. In this situation, the critical behavior should be confirmed by scaling analysis of the alternating susceptibility, which is addressed below.

2. Alternating magnetic susceptibility

The SSG can also be revealed by the study of dynamical response obtained from the temperature dependence of alternating (AC) susceptibility studied at various frequencies. This study was performed for Fe_3O_4-PP from 4.5 to 300 K for excitation frequencies in the nominal range 0.3 Hz − 1 kHz and the obtained real and imaginary components are presented in Figs. 6(a) and 6(b). The system was cooled down from 300 to 4.5 K in the ZFC regime and AC susceptibility was measured for each excitation frequency. Then the temperature was raised to the next value. Both real and imaginary components $\chi'$and χ'', are characterized by broad maxima which shift to higher temperatures with increasing excitation frequency. The value of the maximum in χ' tends to decrease with increasing excitation frequency, while for χ'' the opposite trend was found. The behavior of AC susceptibility can be classified using the empirical quantity [15],

$$\Gamma = \frac{\Delta T_m}{T_m \Delta(\log_{10}\omega)}, \tag{2}$$

in which ω stands for the excitation frequency, T_m denotes the position of the peak in χ', and ΔT_m represents a change of T_m with changing the frequency. Whereas for SPM systems without magnetic interactions $\Gamma \approx 0.3$ may be anticipated [13], $\Gamma \approx 0.0045$–0.06 was reported in systems in which the existence of spin glass or SSG was proved [24,34]. The value of Γ for Fe_3O_4-PP estimated as $\Gamma \approx 0.06$ suggests that the studied system represents SSG rather than SPM.

Following established convention [17,34] T_m was assigned to the freezing temperature T_f for each excitation frequency. Subsequently, $T_f(\omega)$ was used to construct the temperature dependence of the relaxation time τ and the results are presented in Figs. 6(c) and 6(d). In the first approximation, neglecting the magnetic coupling among nanoparticles, the data were analyzed using the Arrhenius formula,

$$\tau(T) = \tau_0 \exp(E_a/k_B T), \tag{3}$$

in which τ_0 represents a characteristic relaxation time; E_a and k_B denote the energy barrier and Boltzmann constant, respectively. Despite the reasonable agreement with the data, the obtained value of $\tau_0 = (2.9 \pm 1.3) \times 10^{-24}$ s significantly differs from $\tau_0 \approx 10^{-8}$ s as anticipated for weakly or non-interacting nanoparticle systems [21]; similarly, the resultant value of the energy barrier $E_a/k_B = (128 \pm 9.3) \times 10^2$ K is

difficult to accept. In the next step, magnetic coupling was taken into account and the SSG scenario was considered. Spin-glass and SSG systems are characterized by the creation of clusters consisting of magnetic moments frozen in random directions. The magnetic correlation length associated with the size of the clusters becomes a function of time and temperature depending on the experimental conditions and so does the energy barrier [35]. Slowing down the dynamic response upon cooling toward glassy temperature T_g in 3D spin glass may be described by the power law,

$$\tau(T) = \tau_0 \left(\frac{T}{T_g} - 1 \right)^{-z\upsilon}, \tag{4}$$

in which υ represents the critical exponent for the correlation length $\xi[\xi(T) \approx \varepsilon^{-\upsilon}$, $\varepsilon = (T/T_g - 1)]$ and z stands for the critical index involved in dynamical-scaling theory $[\tau(T) \approx \xi^z]$. The analysis for $T_g = 211\,\mathrm{K}$ yielded $\tau_0 = 2 \times 10^{-8}$ s suggesting clusterlike relaxation. The obtained value of $z\upsilon = 8.6 \pm 0.46$ agrees well with $z\upsilon = 8.2 \pm 1.0$ reported for SSG found in closed-packed Fe_3O_4 nanoparticles [24]. Notably, SSG was reported also in other 3D Fe_3O_4 systems, namely, for Fe_3O_4 nanoparticles prepared by the coprecipitation technique and coated by the SiO_2 layer, in which the analysis using critical slowing down led to $\tau_0 = 8.7 \times 10^{-6}$ s, $z\upsilon = 11.9 \pm 0.01$, and $T_g = 97.6\,\mathrm{K}$ [26]. Alternatively, using the same approach for small bare Fe_3O_4 nanoparticles prepared by the coprecipitation technique yielded $\tau_0 = 3.9 \times 10^{-11}$ s, $z\upsilon = 7.9$, and $T_g = 112\,\mathrm{K}$ for nanoparticles with 2.5 nm diameter [27]. However, in this system SSG was proposed to arise due to spin canting and the formation of the glassy state on the surface of nanoparticles. The conjecture was supported by gradual decreasing of the effect with increasing the size of Fe_3O_4 nanoparticles. Consequently, it may be stated that the results of the analysis of the AC susceptibility seem to support the SSG scenario in Fe_3O_4-PP which is governed by interparticle interactions rather than properties of their surface.

Alternatively, AC susceptibility data were analyzed using the prediction for 2D spin glass. More specifically, the prediction for Ising spins on a square lattice with random bonds and bimodal distribution of the nearest-neighbor exchange coupling was used as a limiting model which is, to the best of our knowledge, the only available prediction for 2D spin glasses. Within this model, the temperature dependence of the relaxation time is given by

$$\tau(T) = \tau_0 \exp[(b/T)^{1+\psi\alpha}], \tag{5}$$

in which b scales the energy barrier; coefficients ψ and α are exponents for the size dependence of the energy barrier and temperature dependence of the correlation length, respectively. The analysis yielded $\tau_0 = (4.1 \pm 0.3) \times 10^{-38}$ s, $b = 2280 \pm 102\,\mathrm{K}$, and $\psi\alpha = 0.6 \pm 0.25$. However, the obtained values significantly differ from those found in 2D spin glasses with a bimodal distribution of exchange couplings [15]; the value of τ_0 is even not physically acceptable. It should be stressed that even excellent agreement between the data and the predictions for the temperature dependence of the relaxation time with physically acceptable values of parameters may not be conclusive regarding the value of the critical temperature. Full dynamic scaling of the absorption

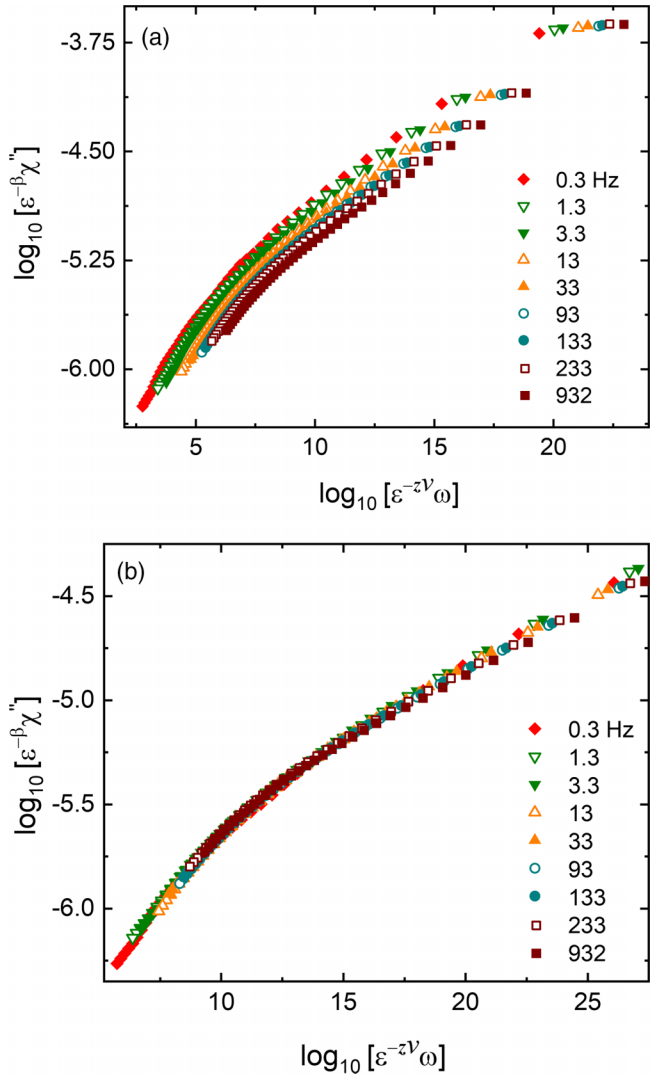

FIG. 7. Dynamical scaling analysis of $\chi''(T, \omega)$ for $T > T_g$ using Eq. (6) and (a) $T_g = 211\,\mathrm{K}$, $z\upsilon = 8.6$, $\beta = 1$, and (b) $T_g = 225\,\mathrm{K}$, $z\upsilon = 13$, $\beta = 0.8$.

component of AC susceptibility can confirm critical dynamics in the studied system. The scaling is based on the prediction that the behavior of the imaginary component of AC susceptibility in a linear regime may be described as follows,

$$\chi''(T, \omega) = \varepsilon^{\beta} F(\omega \varepsilon^{-z\upsilon}), \tag{6}$$

where the function $F(x)$ asymptotically behaves as $F(x) \approx x^{\beta/z\upsilon}$. Parameter β is a critical exponent for the autocorrelation function with $\beta = 1$ in the mean-field approximation [15]. Critical dynamics should be manifested by the universal behavior of the data using the full scaling relation [Eq. (6)]. However, using the values of parameters $T_g = 211\,\mathrm{K}$ and $z\upsilon = 8.6$ obtained from the analysis of potential critical behavior in the framework of the de Almeida and Thouless model [Eq. (1)] and critical slowing down [Eq. (4)], respectively, and taking $\beta = 1$ no universality could be obtained; see Fig. 7(a). Alternation of the values of β did not change the situation significantly. On the other hand, the excellent

universal behavior of the data was found after pronounced renormalization of the T_g and $z\upsilon$ parameters; see Fig. 7(b).

The observed behavior is fully consistent with the well-known fact about applying scaling relations appropriate for 3D systems with $T_c \neq 0$ to 2D spin glasses with bimodal interactions which were proved to be noncritical. In these systems cusps in AC susceptibility are associated with freezing, but not with critical phenomena [15]. Consequently, the necessity of large renormalization of parameters for obtaining collapse in dynamic scaling using Eq. (6) together with questionable values of both critical temperature and the width of the distribution of exchange interactions in Fe_3O_4-PP from the analysis based on the de Almeida and Thouless model might suggest a deviation toward 2D magnetic behavior. In this context, it may be mentioned that even if critical slowing down analysis for nonzero T_c and reasonable value of $z\upsilon$ yield excellent agreement with the data, the absence of universality in AC susceptibility may still suggest that the studied system is not critical [36]. The indicated deviation from 3D magnetic behavior in Fe_3O_4-PP stimulated further dynamic scaling of AC susceptibility data using the equation

$$\chi''(T,\omega)T^{1+\gamma-\psi\alpha} = F[-\ln(\omega\tau_0)T^{\psi\alpha}], \tag{7}$$

in which γ represents the critical index for nonlinear susceptibility. The formula was proposed for a 2D magnetic system of Ising spins on the square lattice with random bonds and bimodal distribution of the nearest-neighbor exchange coupling, whose dynamics is noncritical [37]. The analysis revealed the absence of universal behavior for arbitrary sets of parameters. This fact does not support the results of the critical slowing down analysis using the prediction for the considered 2D magnetic system. However, the obtained result may not be surprising since, unlike in the model, Fe_3O_4-PP is characterized by dominant dipolar coupling with more complexity than the bimodal distribution of the magnitudes of the interactions and random location of nanoparticles/aggregates on the substrate. Consequently, it may be stated that although the analyses of static and alternating susceptibilities support the formation of SSG in the studied system unambiguous determination of its magnetic dimensionality remains an open question.

3. *Memory and aging effects*

Further support for forming SSG in Fe_3O_4-PP may be searched in the investigation of aging, memory, and rejuvenation phenomena which belong to nonequilibrium magnetization dynamics of both spin-glass and SSG systems [24]. The experimental investigation of the aging phenomenon may be based on cooling the system in a low magnetic field from a high enough temperature (i.e., $T \gg T_g$) to a selected temperature $T_{\text{meas}} < T_g$, where the system is kept for a waiting time t_w and aged. Subsequently, the magnetic field is turned off and the time dependence of the remanent magnetization is recorded. The response function $S(t) = (1/M_0)[\partial M/\partial \log(t)]$ vs $\log(t)$ is for $t \approx t_w$ characterized by a round maximum; such a behavior was indeed found in various spin-glass and SSG systems [38,39]. However, since the response function $S(t)$ of SSG has the same features also for SPM with the distribution of sizes of nanoparticles as predicted in Ref. [22], studies of the aging effect using the aforementioned

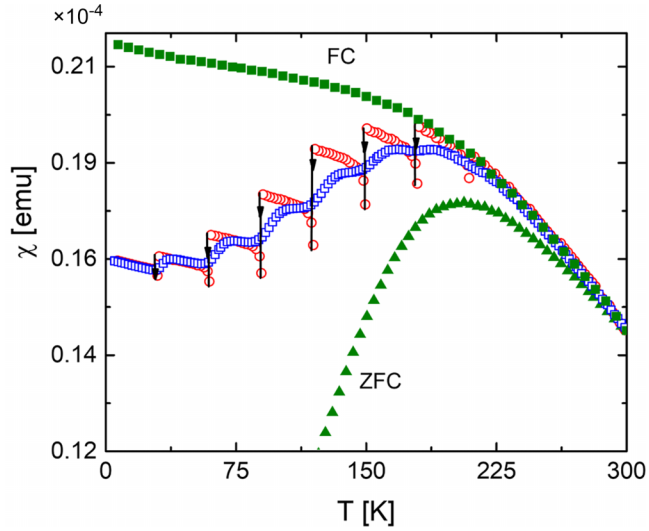

FIG. 8. Temperature dependence of the reference FC susceptibility $\chi_{\text{FC}}^{\text{Ref}}$ (filled green squares), FC susceptibilities obtained during cooling $\chi_{\text{FC}}^{\text{Cool}}$ (open red circles) and heating $\chi_{\text{FC}}^{\text{Heat}}$ (open blue squares) respectively, and ZFC susceptibility χ_{ZFC} (filled green upward triangles) of Fe_3O_4-PP in magnetic field 10 Oe. See the text for a more detailed discussion.

response function were not performed in Fe_3O_4-PP. Alternatively, the memory effect represents a very informative tool in distinguishing the nature of the low-energy states in disordered systems. Adopting the nomenclature from the Ref. [24] memory effect was for Fe_3O_4-PP investigated using *genuine* FC measurement: the sample was cooled from 300 K in magnetic field $H = 10$ Oe to intermediate temperatures $T_i = 180$, 150, 120, 90, 60, and 30 K; see Fig. 8. After arriving to the given T_i the magnetic field was switched off and the sample was aged for $t_s = 3600$ s. Subsequently, the magnetic field was switched on ($H = 10$ Oe) and the sample was cooled to the next T_i. During the cooling and intermediate stops at T_i susceptibility $\chi_{\text{FC}}^{\text{Cool}}$ was measured. Immediately after reaching the minimum temperature 10 K, the sample was continuously heated to 300 K in magnetic field $H = 10$ Oe and the susceptibility $\chi_{\text{FC}}^{\text{Heat}}$ was monitored. Below T_g, temperature dependence of $\chi_{\text{FC}}^{\text{Cool}}$ starts to deviate significantly from the reference FC susceptibility $\chi_{\text{FC}}^{\text{Ref}}$ [Figs. 4(a) and 4(b)] obtained in a continuous regime. While $\chi_{\text{FC}}^{\text{Cool}}$ increases upon cooling between intermediate temperatures T_i, during aging at each T_i, time dependence of $\chi_{\text{FC}}^{\text{Cool}}$ suggests the tendency of development toward a disordered and nonmagnetic state. Temperature dependence of the susceptibility investigated upon heating in a magnetic field $\chi_{\text{FC}}^{\text{Heat}}$ displays a staircaselike pattern, where steps are located close to each T_i and become less pronounced for higher T_i. The observed dependence confirms the memory effect, where the spin configurations successively imprinted at each T_i during cooling are retrieved while heating back to 300 K.

Nevertheless, the memory effect can also be observed in SPM with the distribution of nanoparticle volumes. For SPM, the staircaselike pattern in the $\chi_{\text{FC}}^{\text{Heat}}$ curve persists, but, unlike in Fe_3O_4-PP, $\chi_{\text{FC}}^{\text{Heat}}$ is increasing with decreasing temperature [22]. The observed behavior (Fig. 8), which qualitatively

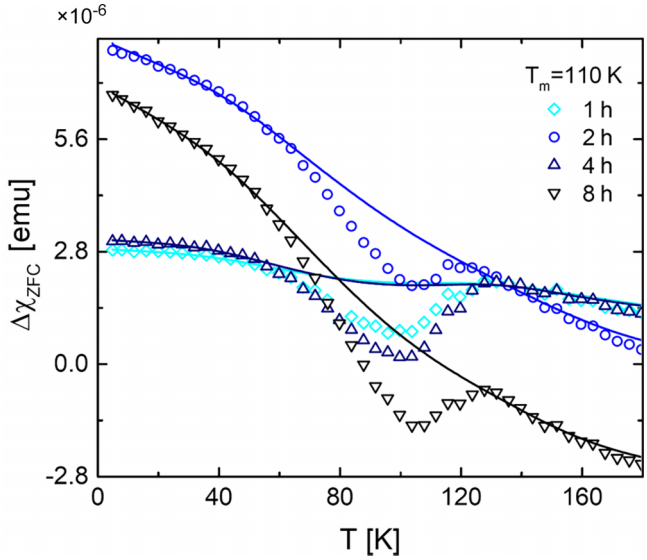

FIG. 9. Temperature dependence of the quantity $\Delta\chi_{\mathrm{ZFC}} = \chi^{W}_{\mathrm{ZFC}} - \chi^{\mathrm{Ref}}_{\mathrm{ZFC}}$ of Fe_3O_4-PP for diffent waiting times. The corresponding estimations for the baseline, χ^{W}_{B}, are denoted by solid lines. See the text for a more detailed discussion.

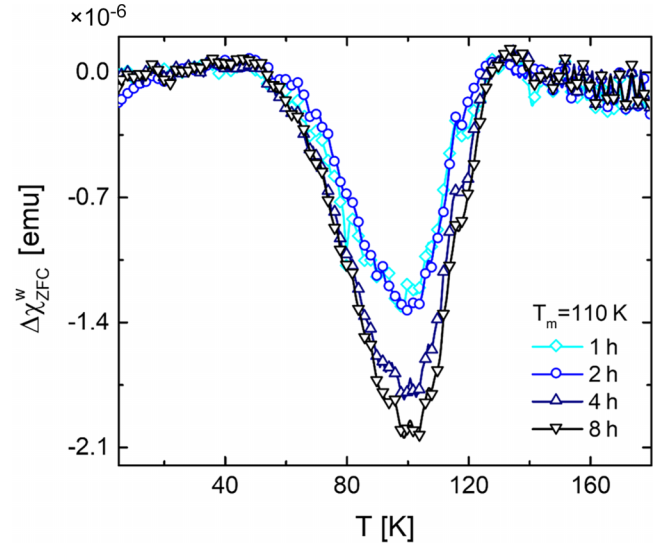

FIG. 10. Temperature dependence of $\Delta\chi^{W}_{\mathrm{ZFC}}$ of Fe_3O_4-PP for different waiting times. See the text for a more detailed discussion.

agrees with the prediction given by the so-called random-energy model for SSG [40] and was found in other SSG systems [22,41,42], could be considered as strong support for the onset of SSG in Fe_3O_4-PP. However, it should be stressed that even though the shape of the staircaselike pattern in $\chi^{\mathrm{Heat}}_{\mathrm{FC}}$ may display the tendency to increase upon heating it still cannot be considered as final evidence of SSG formation in a studied system. Such a situation was demonstrated in [29], in which $\chi^{\mathrm{Heat}}_{\mathrm{FC}}$ of a Fe_3O_4 nanoparticle system did posses the aforementioned feature, yet ZFC measurement did not confirm the existence of the so-called aging dip; consequently, the existence of SSG was not confirmed.

Genuine ZFC measurement represents another approach for studying the aging effect. It enables us to distinguish between SSG and SPM since a characteristic so-called aging dip in ZFC susceptibility exists only in SSG systems [24]. This effect was investigated by ZFC for Fe_3O_4-PP from 300 to 5 K in a zero magnetic field. When the temperature reached the selected value $T_m \approx 0.5T_g$, $T_m = 110\,\mathrm{K}$, the sample was isothermally aged during various waiting times t_w. Subsequently, ZFC continued to 5 K. Immediately after the minimum temperature was reached the sample was reheated and susceptibility in magnetic field 10 Oe, χ^{w}_{ZFC}, was monitored upon reheating. In addition, the reference susceptibility curve $\chi^{\mathrm{Ref}}_{\mathrm{ZFC}}$ obtained by ZFC cooling without any stop was recorded as well. The spin configuration of SSG is assumed to develop toward an equilibrium state during t_w. The equilibrated spin configuration becomes frozen upon further cooling and is retrieved during subsequent heating to T_m. Experimentally, the aging is manifested as a dip in quantity $\Delta\chi_{\mathrm{ZFC}} = \chi^{\mathrm{W}}_{\mathrm{ZFC}} - \chi^{\mathrm{Ref}}_{\mathrm{ZFC}}$ (see Fig. 9) which in SSG, for a constant value of the temperature T_m, becomes more pronounced with increasing waiting time t_w. It was found that a small difference between $\chi^{\mathrm{Ref}}_{\mathrm{ZFC}}$ and $\chi^{\mathrm{W}}_{\mathrm{ZFC}}$ for various t_w persisted in a wide temperature range. The origin of this effect has not been fully clarified; tentatively it is assumed to arise from the not fully reversible motion of the agglomerates on the substrate upon thermal cycling during performance of the selected protocol. Obviously, such a motion can be much more significant in Fe_3O_4-PP than for nanoparticles deposited, e.g., on glass, or Al_2O_3 due to pronounced differences in the values of the coefficient of thermal expansion $\alpha(\alpha_{\mathrm{PP}} = 120 \times 10^{-6}\,\mathrm{K}^{-1}$, $\alpha_{\mathrm{glass}} = 7 \times 10^{-7}\,\mathrm{K}^{-1}$, $\alpha_{\mathrm{Al_2O_3}} = 8 \times 10^{-6}\,\mathrm{K}^{-1})$. However, even with the aforementioned feature the dip characteristic for aging and rejuvenation can still be unambiguously distinguished around $T_m = 110\,\mathrm{K}$. In order to compare the depth of the dip for various t_w, a baseline for the susceptibility difference, χ^{W}_{B}, was determined by fitting a polynomial of the sixth degree to $\Delta\chi_{\mathrm{ZFC}}$ for temperatures below 50 K and above 150 K. Data in these temperature regimes were considered to be outside the region of the dip. Separate estimates for χ^{W}_{B} were determined for each waiting time, and the estimates are shown in Fig. 9. The quantities $\Delta\chi^{\mathrm{W}}_{\mathrm{ZFC}} = \chi^{\mathrm{W}}_{\mathrm{ZFC}} - \chi^{W}_{B}$, representing the form and depth of the dips, are plotted in Fig. 10.

As can be seen, the obtained results confirm the expected tendency of growing the depth of the dip with increasing t_w, which is a feature anticipated exclusively in SSG.

A question might arise of what the key factors are that govern the formation of SSG in nanoscopic systems. The width of the distribution of magnetic interactions may be considered. Similarly as in the pioneering work of Sherrington and Kirkpatrick [10], in which sufficiently wide Gaussian distribution of exchange coupling was found to be necessary for forming spin-glass in a 3D Ising ferromagnet, nanoscopic systems with a wider distribution of particle size tend to form SSG, whereas SPM may be anticipated for nanoparticles of the same size and narrow size distribution [29]. In addition, distances among nanoparticles determining the magnitude of dipolar coupling should be adequately shorter and these can be, to some extent, controlled by a method of preparation. More specifically, systematic study of structural and magnetic properties of 5 nm citric acid capped $CoFe_2O_4$ nanoparticles

synthesized by the coprecipitation method under different *p*H conditions revealed that whereas the size of the nanoparticles remains nominally the same, the distances among them as well as their ability to form clusters are strongly affected by *p*H values, which leads to pronounced differences in their magnetic response [43].

As mentioned above, the appearance of SSG requires sufficiently strong magnetic coupling among nanoparticles. For example, it has been clarified that for the assembly of Fe_2O_3 nanoparticles with 11 nm diameter and nominally 15 − 18 nm distance, in which SSG was formed, the ratio of dipolar-interaction energy and single-particle anisotropy was $J_{\rm dip}/E_a \approx 0.1$ [44]. In this context, the question might arise about the estimation of the ratio of dipolar coupling within the layer $J_{\rm dip}^{\rm intra}$ of nanoparticles and the interaction among the wrapped layers, $J_{\rm dip}^{\rm inter}$. Depending on the strength of dipolar interaction for closed-packed systems various theoretical models were proposed, for example, the Dormann-Bessais-Fiorani model [45] or the Mørup-Tronc model [46], to incorporate the effect of dipolar coupling into the dynamic response. However, for reliable quantitative analysis, detailed knowledge of the local surroundings of a magnetic nanoparticle is needed, which for $J_{\rm dip}^{\rm intra}$ in Fe_3O_4-PP is not directly available. In addition, even the determination of the total magnetic moment of a given agglomerate in low magnetic fields may not be straightforward due to the distribution of sizes of nanoparticles and the potential coexistence of ferro- and antiferromagnetic couplings within the agglomerate, as well as randomness in easy-axis orientations of nanoparticles within the agglomerate. On the other hand, considering a single 10 nm Fe_3O_4 nanoparticle, the analysis of magnetization curves by a multimodal Langevin fit [47,48] enables the estimation of its magnetic moment as 390 μ_B. Subsequently, taking into account the dipolar nature of magnetic coupling, $J_{\rm dip} \sim 1/r^3$, as well as a resultant thickness of the paper and foil among the wrapped layers of 150 μm, the magnitude of dipolar coupling for 10 nm nanoparticles between the wrapped layers can be estimated as $J_{\rm dip}^{\rm inter}/k_B \approx 10^{-12}$ K. Obviously, such an extremely low value of magnetic interaction cannot be responsible for the magnetic response observed at nominally 200 K. However, the contributions of larger clusters still need to be clarified. Consequently, assemblies with tailored composition and size of the aggregates will be prepared and corresponding experimental studies will be conducted. Alternation of the size of the nanoparticles and their mutual distance, as well as the size of agglomerates, will be performed to investigate the influence of the distribution of nanoparticles on the existence and the value of T_g. In addition, the measurement of the local magnetic response of a single agglomerate is in preparation.

IV. CONCLUSION

Structural characterization and the investigation of static and dynamic magnetic properties of a two-dimensional assembly consisting of aggregated Fe_3O_4 nanoparticles of nominal size 10 nm deposited on a plasma-treated polypropylene substrate were performed. The deposited nanoparticles create agglomerates with a wide distribution of sizes ranging from ≈10 to ≈400 nm. The evaluation of static susceptibility using the de Almeida and Thouless model suggested the formation of SSG at $T_g \cong 210$ K. Relative shift of the maximum in alternating susceptibility $\Gamma \approx 0.06$ and $z\upsilon = 8.6$ obtained from critical slowing down analysis suggest the onset of SSG in the studied system. This suggestion was further supported by the investigation of memory and aging effects using genuine FC and ZFC protocols which were found to be fully consistent with other reported SSG systems. The necessity of large renormalization of parameters for obtaining the universal behavior of the data in dynamic scaling of alternating susceptibility together with questionable values of both critical temperature and the width of the distribution of exchange interactions from the analysis based on the de Almeida and Thouless model may indicate deviation toward 2D magnetic behavior. In addition, the interplanar dipolar interaction for individual 10 nm Fe_3O_4 nanoparticles in the used assembly can be suggested as negligible. The obtained results suggest that the studied assembly may be appropriate for investigating the conditions of SSG formation in systems with a more complex distribution of magnetic couplings and, potentially, for creating an alternative model system of 2D SSG with dominant dipolar coupling.

ACKNOWLEDGMENTS

We would like to thank P. Hrubovčák for expert technical help. This work was supported by the Slovak Research and Development Agency under Projects No. APVV-18–0197 and No. GACR No. 21–02550S, and by the OP VVV Project NANOTECH ITI II. No. CZ.02.1.01/0.0/0.0/18_069/0010045 (for Z.K. and V.S.).

[1] F. Tian, K. Cao, Y. Zhang, Y. Zeng, R. Zhang, T. Chang, Ch. Zhou, M. Xu, X. Song, and S. Yang, Sci. Rep. **6**, 30801 (2016).
[2] J. Ye, T. Baldauf, S. Mattauch, N. Paul, and A. Paul, Commun. Phys. **2**, 114 (2019).
[3] H. Gabold, Z. Luan, N. Paul, M. Opel, P. Můller-Buschbaum, M. Law, and A. Paul, Sci. Rep. **8**, 4835 (2018).
[4] M. Perovic, M. Boskovic, V. Kusigerski, Z. Jaglicic, J. Blanusa, V. Spasojevic, N. Pizurova, and O. Schneeweiss, J. Alloys Compd. **855**, 157523 (2021).
[5] M. Vasilakaki, G. Margaris, D. Peddis, R. Mathieu, N. Yaacoub, D. Fiorani, and K. Trohidou, Phys. Rev. B **97**, 094413 (2018).
[6] D. Peddis, K. N. Trohidou, M. Vasilakaki, G. Margaris, M. Bellusci, F. Varsano, M. Hudl, N. Yaacoub, D. Fiorani, P. Nordblad, and R. Mathieu, Sci. Rep. **11**, 7743 (2021).
[7] M. Saccone, A. Scholl, S. Velten, S. Dhuey, K. Hofhuis, C. Wuth, Y.-L. Huang, Z. Chen, R. V. Chopdekar, and A. Farhan, Phys. Rev. B **99**, 224403 (2019).

[8] S. C. Skjærvø, Ch. H. Marrows, R. L. Stamps, and L. J. Heyderman, Nat. Rev. Phys. **2**, 13 (2020).

[9] A. P. Ramirez, A. Hayashi, R. J. Cava, R. Siddhartan, and B. S. Shastry, Nature (London) **399**, 333 (1999).

[10] D. Sherrington and S. Kirkpatrick, Phys. Rev. Lett. **35**, 1792 (1975).

[11] K. Binder and A. P. Young, Rev. Mod. Phys. **58**, 801 (1986).

[12] R. N. Bhatt and A. P. Young, Phys. Rev. Lett. **54**, 924 (1985).

[13] A. K. Hartmann and A. P. Young, Phys. Rev. B **64**, 180404(R) (2001).

[14] N. Kawashima and H. Rieger, Europhys. Lett. **39**, 85 (1997).

[15] J. A. Mydosh, *Spin Glasses: An Experimental Introduction* (CRC Press, London, 1993), and references therein.

[16] C. Dekker, A. Arts, and H. W. Dewijn, J. Phys. France **49**, C8-1013 (1988).

[17] L. Hoines, R. Stubi, R. Loloee, J. A. Cowen, and J. Bass, Phys. Rev. Lett. **66**, 1224 (1991).

[18] J. A. Olive, A. P. Young, and D. Sherrington, Phys. Rev. B **34**, 6341 (1986).

[19] J. N. Graham, M. J. Coak, S. Son, E. Suard, J.-G. Park, L. Clark, and A. R. Wildes, Phys. Rev. Mater. **4**, 084401 (2020).

[20] S. Lupínková, M. Benkocká, P. Ryšánek, and Z. Kolská, Polym. Eng. Sci. **62**, 1463 (2022).

[21] A. Rajan, M. Sharma, and N. K. Sahu, Sci. Rep. **10**, 15045 (2020).

[22] M. Sasaki, P. E. Jönsson, H. Takayama, and H. Mamiya, Phys. Rev. B **71**, 104405 (2005).

[23] S. Nakamae, Y. Tahri, C. Thibierge, D. L. Hôte, E. Vincent, V. Dupuis, E. Dubois, and R. Perzynski, J. Appl. Phys. **105**, 07E318 (2009).

[24] M. Suzuki, S. I. Fullem, I. S. Suzuki, L. Wang, and Ch. J. Zhong, Phys. Rev. B **79**, 024418 (2009).

[25] D. Peddis, C. Cannas, A. Musinu, and G. Piccaluga, J. Phys. Chem. C **112**, 5141 (2008).

[26] W. S. Torres, A. S. Alcantara, R. D. Bini, M. B. Alvim, M. C. Santos, L. F. C´otica, and D. L. Rocco, Mater. Chem. Phys. **290**, 126511 (2022).

[27] B. Aslibeiki, M. H. Ehsani, F. Nasirzadeh, and M. A. Mohammadi, Mater. Res. Express **4**, 075051 (2017).

[28] R. Revathy, M. R. Varma, and K. P. Surendran, Phys. Status Solidi B **258**, 2000341 (2020).

[29] A. Ch. Gandhi, P. M. Reddy, T. S. Chan, Y. P. Ho, and S. Y. Wu, RSC Adv. **5**, 84782 (2015).

[30] J. R. L. de Almeida and D. J. Thouless, J. Phys. Math. Gen. **11**, 983 (1978).

[31] S. Sahoo, O. Petracic, Ch. Binek, W. Kleemann, J. B. Sousa, S. Cardoso, and P. P. Freitas, Phys. Rev. B **65**, 134406 (2002).

[32] D. H. Manh, P. T. Phong, L. H. Nguyen, D. K. Tung, N. X. Phuc, and I. J. Lee, J. Magn. Magn. Mater. **368**, 240 (2014).

[33] G. Toulose and M. Gabay, J. Phys. Lett. **42**, 103 (1982).

[34] P. Hrubovčák, A. Zeleňáková, V. Zeleňák, D. Peddis, and D. Fiorani, Phys. Rev. B **102**, 024433 (2020).

[35] J. P. Bouchard, V. Dupuis, J. Hammann, and E. Vincent, Phys. Rev. B **65**, 024439 (2001).

[36] M. F. Hansen, P. E. Jönsson, P. Nordblad, and P. Svedlindh, J. Phys.: Condens. Matter **14**, 4901 (2002).

[37] C. Dekker, A. F. M. Arts, H. W. de Wijn, A. J. van Duyneveldt, and J. A. Mydosh, Phys. Rev. B **40**, 11243 (1989).

[38] S. Sahoo, O. Petracic, W. Kleemann, P. Nordblad, S. Cardoso, and P. P. Freitas, Phys. Rev. B **67**, 214422 (2003).

[39] M. S. Andersson, J. A. de Toro, S. S. Lee, R. Mathieu, and P. Nordblad, Europhys. Lett. **108**, 17004 (2014).

[40] M. Sasaki and K. Nemoto, J. Phys. Soc. Jpn. **69**, 3045 (2000).

[41] M. S. Andersson, J. Nanosci. Nanotechnol. **19**, 4903 (2019).

[42] H. Khurshid, P. L. Kelley, Ò. Iglesias, J. Alonso, M. H. Phan, Ch. J. Sun, M. L. Saboungi, and H. Shrikanth, Sci. Rep. **5**, 15054 (2015).

[43] Ľ. Nagy, A. Zeleňáková, P. Hrubovčák, M. Barutiak, M. Lisnichuk, J. Bednarčík, J. Vargová, R. Jendželovský, J. Ševc, and Š. Vilček, J. Alloys Compd. **960**, 170833 (2023).

[44] K. Hiroi, K. Komatsu, and T. Sato, Phys. Rev. B **83**, 224423 (2011).

[45] J. L. Dormann, L. Bessais, and D. Fiorani, J. Phys. C: Solid State Phys. **21**, 2015 (1988).

[46] S. Mørup, Europhys. Lett. **28**, 671 (1994).

[47] F. C. Fonseca, G. F. Goya, R. F. Jardim, R. Muccillo, N. L. V. Carreño, E. Longo, and E. R. Leite, Phys. Rev. B **66**, 104406 (2002).

[48] M. Tadic, V. Kusigerski, D. Markovic, I. Milosevic, and V. Spasojevic, J. Magn. Magn. Mater. **321**, 12 (2009).